Structural Basis for Substrate Specificity in Phosphate Binding $(\beta/\alpha)_8$-Barrels: D-Allulose 6-Phosphate 3-Epimerase from *Escherichia coli* K-12[†,‡]

Kui K. Chan,[§] Alexander A. Fedorov,[||] Elena V. Fedorov,[||] Steven C. Almo,*[,||] and John A. Gerlt*[,§]

Departments of Biochemistry and Chemistry, University of Illinois at Urbana−Champaign, 600 South Mathews Avenue, Urbana, Illinois 61801, and Department of Biochemistry, Albert Einstein College of Medicine, 1300 Morris Park Avenue, Bronx, New York 10461

Received May 6, 2008; Revised Manuscript Received July 12, 2008

ABSTRACT: Enzymes that share the $(\beta/\alpha)_8$-barrel fold catalyze a diverse range of reactions. Many utilize phosphorylated substrates and share a conserved C-terminal $(\beta/\alpha)_2$-quarter barrel subdomain that provides a binding motif for the dianionic phosphate group. We recently reported functional and structural studies of D-ribulose 5-phosphate 3-epimerase (RPE) from *Streptococcus pyogenes* that catalyzes the equilibration of the pentulose 5-phosphates D-ribulose 5-phosphate and D-xylulose 5-phosphate in the pentose phosphate pathway [J. Akana, A. A. Fedorov, E. Fedorov, W. R. P. Novack, P. C. Babbitt, S. C. Almo, and J. A. Gerlt (2006) *Biochemistry 45,* 2493−2503]. We now report functional and structural studies of D-allulose 6-phosphate 3-epimerase (ALSE) from *Escherichia coli* K-12 that catalyzes the equilibration of the hexulose 6-phosphates D-allulose 6-phosphate and D-fructose 6-phosphate in a catabolic pathway for D-allose. ALSE and RPE prefer their physiological substrates but are promiscuous for each other's substrate. The active sites (RPE complexed with D-xylitol 5-phosphate and ALSE complexed with D-glucitol 6-phosphate) are superimposable (as expected from their 39% sequence identity), with the exception of the phosphate binding motif. The loop following the eighth β-strand in ALSE is one residue longer than the homologous loop in RPE, so the binding site for the hexulose 6-phosphate substrate/product in ALSE is elongated relative to that for the pentulose 5-phosphate substrate/product in RPE. We constructed three single-residue deletion mutants of the loop in ALSE, ΔT196, ΔS197 and ΔG198, to investigate the structural bases for the differing substrate specificities; for each, the promiscuity is altered so that D-ribulose 5-phosphate is the preferred substrate. The changes in k_{cat}/K_m are dominated by changes in k_{cat}, suggesting that substrate discrimination results from differential transition state stabilization. In both ALSE and RPE, the phosphate group hydrogen bonds not only with the conserved motif but also with an active site loop following the sixth β-strand, providing a potential structural mechanism for coupling substrate binding with catalysis.

The $(\beta/\alpha)_8$-barrel (or TIM[1]-barrel) fold is the most common fold in the PDB database (*1, 2*). The most recent SCOP database (http://scop.mrc-lmb.cam.ac.uk/scop/; Release 1.73, November 2007) lists 33 "superfamilies" that contain a domain with the $(\beta/\alpha)_8$-barrel fold. Most are enzymes that catalyze a diverse range of reactions. Seven of the "superfamilies" contain structurally conserved motifs for binding the phosphate group of a phosphorylated substrate; almost always, this motif is located at the ends of the seventh and eighth β-strands of the domain.

Sterner and Wilmanns and co-workers first provided evidence that the $(\beta/\alpha)_8$-barrel fold evolved from smaller subdomains (*3*). Based on both sequence and structures, they noted that two enzymes in the histidine biosynthetic pathway, phosphoribosylformimino-5-aminoimidazole carboxamide ribonucleotide isomerase (HisA) and imidazole glycerolphosphate synthase (HisF), are formed by two tandem copies of a $(\beta/\alpha)_4$-half-barrel that form the intact $(\beta/\alpha)_8$-barrel. Sterner and co-workers later demonstrated that the N- and C-terminal $(\beta/\alpha)_4$-half-barrels of HisF from *Thermotoga maritima* could be separately expressed as stable, folded proteins (*4*). The substrates for both HisA and HisF contain two phosphate groups, with both $(\beta/\alpha)_4$-half-barrels containing a conserved phosphate binding motif (at the ends of the third and fourth and, also, the seventh and eighth β-strands in the complete $(\beta/\alpha)_8$-barrel) (*5*).

[†] This research was supported by Grant GM-65155 from the National Institutes of Health.

[‡] The X-ray coordinates and structure factors for ALSE complexed with (1) sulfate anion and Mg^{2+} and (2) D-glucitol 6-phosphate and Mg^{2+} have been deposited in the Protein Data Bank (PDB accession codes 3CT7 and 3CTL, respectively).

* To whom correspondence should be addressed. J.A.G.: Department of Biochemistry, University of Illinois, 600 S. Mathews Avenue, Urbana, IL 61801. Phone: (217) 244-7414. Fax: (217) 244-6538. E-mail: j-gerlt@uiuc.edu. S.C.A.: Department of Biochemistry, Albert Einstein College of Medicine, 1300 Morris Park Avenue, Bronx, New York 10461. Phone: (718) 430-2746. Fax: (718) 430-8565. E-mail: almo@aecom.yu.edu.

[§] University of Illinois at Urbana−Champaign.

[||] Albert Einstein College of Medicine.

[1] Abbreviations: HisA, phosphoribosylformimino-5-aminoimidazole carboxamide ribonucleotide isomerase; HisF, imidazole glycerolphosphate synthase; ICP, inductively coupled plasma emission spectroscopy; KGPDC, 3-keto-L-gulonate 6-phosphate decarboxylase; OMPDC, orotidine 5′-monophosphate decarboxylase; RPE, D-ribulose 5-phosphate 3-epimerase; TIM, triose phosphate isomerase; TrpC, indole-3-glycerophosphate synthase; TprF, phosphoribosylanthranilate isomerase.

10.1021/bi800821v CCC: $40.75
Published on Web 08/14/2008

The recognition of a conserved phosphate binding motif allows the suggestion that $(\beta/\alpha)_8$-barrels may be assembled by the modular construction from not only $(\beta/\alpha)_4$-half-barrels but also $(\beta/\alpha)_2$-quarter barrels, thereby allowing the widespread occurrence of the motif in intact $(\beta/\alpha)_8$-barrels domains to be rationalized (*3, 4, 6*−*8*).[2] In indirect support of this possibility, Drennan and co-workers analyzed the sequences and structures of *S*-adenosyl-L-methionine-dependent radical enzymes and predicted the occurrence of enzymes containing $(\beta/\alpha)_4$-half-barrels, $(\beta/\alpha)_6$-three-quarter barrels, and the full $(\beta/\alpha)_8$-barrels, with the number of $(\beta/\alpha)_2$-quarter barrel modules inversely related to the size of the substrate (*9*).

The seven "superfamilies" in SCOP that contain the conserved phosphate binding motif are designated the (1) triose phosphate isomerase (TIM), (2) ribulose-phosphate binding barrel, (3) thiamin phosphate synthase, (4) pyridoxine 5′-phosphate synthase, (5) FMN-linked oxidoreductase, (6) inosine monophosphate dehydrogenase, and (7) PLP-binding barrel "superfamilies". The phosphate-binding motif is located in the C-terminal $(\beta/\alpha)_2$-quarter barrel and is formed from the backbone amides in glycine-rich loops following the seventh and eighth β-strands and the side chain of at least one residue in the loop following the eighth β-strand.

We are interested in understanding structure−function relationships in several members of the functionally diverse "ribulose-phosphate binding barrel" superfamily (*10*). The "superfamily" includes HisA and HisF in the histidine biosynthetic pathway, phosphoribosylanthranilate isomerase (TrpF), indole-3-glycerophosphate synthase (TrpC), and the α-subunit of tryptophan synthase in the tryptophan biosynthetic pathway, orotidine 5′-monophosphate decarboxylase (OMPDC) and 3-keto-L-gulonate 6-phosphate decarboxylase (KGPDC) in the OMPDC suprafamily, a putative *N*-acetylmannosamine 6-phosphate 2-epimerase, and D-ribulose 5-phosphate 3-epimerase (RPE). The diversity of these reactions and the divergent sequences of the members suggest that these are not derived from a common $(\beta/\alpha)_8$-barrel progenitor by the mutational events associated with divergent evolution. Indeed, we concluded that although OMPDC and KGPDC are derived from a common progenitor, they share sequence and structural homology with only the C-terminal $(\beta/\alpha)_2$-quarter barrel in RPE that forms the conserved phosphate binding motif (*10*), consistent with an ancient evolutionary history that involved assembly of these proteins from fractional barrels.

The C-terminal $(\beta/\alpha)_2$-quarter barrel phosphate binding motif provides the structural elements for recognition of the dianionic phosphate group of the substrate. However, the intrinsic binding energy of the phosphate group is used not only to "grip" the substrate but also for catalysis. In the case of TIM, Amyes and Richard compared the rates of isomerization of D-glyceraldehyde 3-phosphate and D-glyceraldehyde and concluded that 84% of the 4×10^{10} enzymatic rate acceleration with the phosphorylated substrate is provided by the intrinsic binding energy of the phosphate group,

Scheme 1

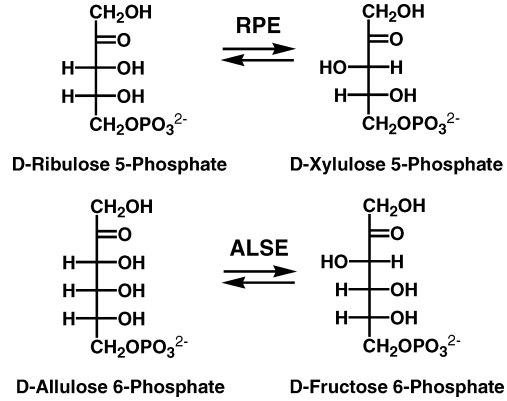

although it is structurally remote from the general basic Glu 165 and the electrophilic His 95 (*11*). In the case of OMPDC, a member of the ribulose-phosphate binding barrel "superfamily", Amyes and Richard reported that phosphite anion accelerates the decarboxylation of a 5′-truncated analogue of OMP that lacks the 5′-phosphomonoester group by a factor of 80000-fold (*12*). Although this factor is a small fraction of the 10^{17} rate acceleration observed with the OMP substrate, the conclusion is that intrinsic binding energy of the remote phosphate group is important for catalysis.

In both TIM (*13*) and OMPDC (*14*), the phosphate group of the substrate not only occupies the conserved phosphate binding motif in the C-terminal $(\beta/\alpha)_2$-quarter barrel but also forms hydrogen bonding interactions with backbone amides and/or side chains in an active site loop, resulting in closure of the loop, exclusion of solvent from the active site, and reorganization of active site functional groups that are directly involved in catalysis. These interactions likely provide the structural mechanism for utilization of the intrinsic binding energy of the phosphate ester group in catalysis (*15*).

We are interested in the role of the phosphate binding motif in ketose phosphate 3-epimerases that are members of the ribulose-phosphate binding barrel "superfamily". RPE catalyzes the 1,1-proton transfer reaction that equilibrates the *pentulose* 5-phosphates D-ribulose 5-phosphate and D-xylulose 5-phosphate in the pentose phosphate pathway (Scheme 1).

Orthologous homologues of RPE catalyze the D-allulose 6-phosphate 3-epimerase reaction (ALSE), a 1,1-proton transfer reaction that equilibrates the *hexulose* 6-phosphates D-allulose (D-psicose) 6-phosphate and D-fructose 6-phosphate (Scheme 1) in a catabolic pathway for D-allose that is encoded by the genomes of several strains of *Escherichia coli* (Scheme 2) (*16*). The D-ribulose 5-phosphate substrate for RPE and the D-allulose 6-phosphate substrate for ALSE differ by a hydroxymethylene group.

We recently reported the structure of the RPE from *Streptococcus pyogenes* liganded with a catalytically essential Zn^{2+} and D-xylitol 5-phosphate, an inert substrate analogue (*10*). In this structure, the 2- and 3-OH groups of the analogue are coordinated to a Zn^{2+}, suggesting that the Zn^{2+} stabilizes the enediolate intermediate generated by abstraction of the 3-proton (Figure 1, panel A). The protein provides four additional ligands for the Zn^{2+}, His 34, His 67, Asp 36, and Asp 176. The substrate analogue directly contacts the protein *via* (1) the 1-OH group that is hydrogen bonded to the amide of Gly 143 in the active site loop following the sixth β-strand,

[2] Modular construction from a $(\beta/\alpha)_2$-quarter barrel that provides the phosphate binding motif does not explain the exclusive occurrence of the motif as the C-terminal $(\beta/\alpha)_2$-quarter barrel of the $(\beta/\alpha)_4$-half-barrels repeated in HisA and HisF and, also, of the large number of complete $(\beta/\alpha)_8$-barrels that contain a single copy of the motif.

Scheme 2

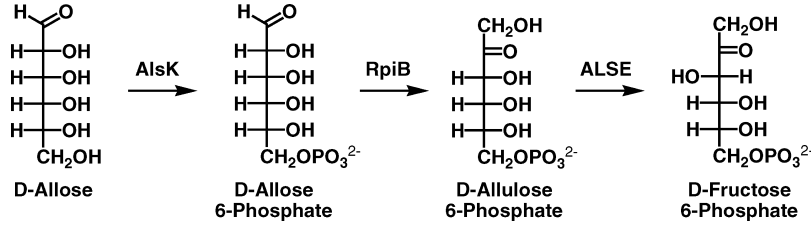

and (2) the 4-OH group that is hydrogen bonded to the OH group of Ser 9 in a loop following the first β-strand. On the basis of this structure, we assigned Asp 36 as the D-ribulose 5-phosphate specific acid/base catalyst and Asp 176 as the D-xylulose 5-phosphate specific acid/base catalyst in the 1,1-proton transfer reaction.

In this structure, the phosphate group of the D-xylitol 5-phosphate ligand is located in the conserved binding motif where it forms hydrogen bonds to the amide of Gly 178 at the end of the seventh β-strand, the amide of Gly 198 at the end of the eighth β-strand, and the OH group of Ser 199 also at the end of the eighth β-strand (Figure 1, panel B). The phosphate group also forms a hydrogen bond with the amide of Gly 146 in the active site loop.

We now report the structure of the ALSE from *E. coli* K-12 in the presence of D-glucitol 6-phosphate, an inert analogue of the D-fructose 6-phosphate product. The phosphate group occupies the phosphate binding motif, which differs from that in RPE by the insertion of a single amino acid residue in the loop following the eighth β-strand. The insertion displaces the position of the binding site for the phosphate group by ~1.5 Å from the binding site for the divalent metal ion relative to the geometry in RPE, thereby forming an elongated site for the phosphorylated hexulose substrate. We kinetically characterized three mutants of ALSE in which a single residue in the loop following the eighth β-strand was deleted, ΔT196, ΔS197 and ΔG198. The values of k_{cat}/K_m, the specificity constant, were significantly increased for the RPE reaction and modestly decreased for the ALSE reaction. That these effects result from changes in the values of k_{cat}, not of K_m, suggests that the specificity constants for RPE and ALSE reflect the ability of the phosphate groups of their substrates to transmit their intrinsic binding energy to the catalytic groups in the active sites, presumably *via* its interactions with the active site loops, and not simply the affinities for the substrates.

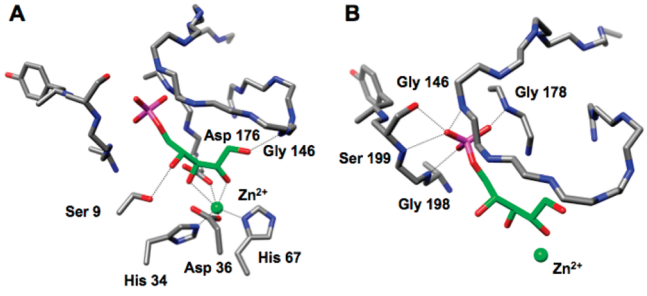

FIGURE 1: The active site of the RPE from *S. pyogenes* (*10*). Panel A, the interactions of the substrate analogue D-xylitol 5-phosphate (green) with the active site. Panel B, the interactions of the phosphate group of D-xylitol 5-phosphate with the phosphate binding motif (Gly 178, Gly 198, and Ser 199) and the active site loop (Gly 146). A 3.2 Å threshold was used for drawing hydrogen bonding and liganding interactions.

MATERIALS AND METHODS

^{1}H NMR and ^{31}P NMR spectra were recorded on a Varian Unity 500NB MHz spectrometer. All compounds used were of the highest available commercial grade.

Preparation of D-Allulose 6-Phosphate. A 50:50 mixture of D-allulose 6-phosphate and D-allose 6-phosphate was prepared from D-allose (Omicron Biochemicals, Inc.) using D-allose kinase (AlsK), a gift from Dr. Brian Miller (*17, 18*), and D-ribose-5-phosphate isomerase B (RpiB).

D-Allose 6-phosphate was prepared from D-allose using AlsK and an ATP regenerating system. D-Allose (5.5 mmol), ATP (0.1 mmol), $MgCl_2$ (1.8 mmol) and acetyl phosphate (4.4 mmol) were dissolved in 200 mL of 50 mM Tris-HCl, pH. 7.6. AlsK (100 U) and acetate kinase (450 U) were added. After the reaction was complete, the enzymes were removed by ultrafiltration, and the solution was applied to a column (2.5 × 25 cm) of DEAE Sepharose Fast Flow (HCO_3^- form) and eluted with a 0 to 1 M linear gradient of triethylammonium bicarbonate, pH 8.2. Fractions containing the product were identified by TLC using the Hanes−Isherwood method and pooled, and triethylammonium bicarbonate was removed by rotary evaporation. ^{1}H and ^{31}P NMR spectra were recorded to verify the identity of the product. ^{1}H NMR (D_2O, 500 MHz): δ 4.72 (d, J = 8.28 Hz, 1H), 4.01 (t, J = 2.98 Hz, 1H), 3.93 (m, 1H), 3.82 (m, 1H), and 3.71 (q, J = 4.77 Hz, 1H). ^{31}P NMR (D_2O, 500 MHz, ^{1}H coupled): 5.66 (t, J = 6.53 Hz).

An equimolar mixture of D-allose 6-phosphate and D-allulose 6-phosphate was prepared from D-allose 6-phosphate using RpiB. RpiB (2 mL of an 80 μM solution) was added to a solution (40 mL) of 1.49 mM D-allose 6-phosphate, 150 mM NaCl, and 50 mM sodium HEPES, pH 7.5. The reaction progress was monitored by removing a 400 μL aliquot, adding 400 μL of D_2O, and recording the ^{31}P NMR spectrum. After the reaction came to equilibrium, RpiB was removed by ultrafiltration. The concentration of D-allulose 6-phosphate was determined by measuring the total phosphate concentration by the Ames method (*19*) and assuming, based on the integration of the ^{31}P NMR spectrum, that 50% of the equilibrated mixture was D-allulose 6-phosphate. ^{31}P NMR (D_2O, 500 MHz coupled): 5.63 (t, J = 6.55 Hz), 5.02 (t, J = 5.39 Hz), and 4.94 (t, J = 5.48 Hz).

Preparation of D-Glucitol 6-Phosphate. D-Glucitol-6-phosphate was prepared by reduction of D-glucose-6-phosphate (7 mmol; Sigma) using $NaBH_4$ (14 mmol) and purified by passing the resulting solution through a column (2.5 × 25 cm) of DEAE Sepharose Fast Flow (HCO_3^- form) and eluting with a 0 to 0.6 M linear gradient of triethylammonium bicarbonate (pH 8.2). Fractions containing product (identified by the Hanes−Isherwood method) were pooled, and triethylammonium bicarbonate was removed by rotary evaporation. ^{1}H, ^{13}C, and ^{31}P NMR spectra were recorded

to verify the product.^{1}H NMR (D_2O, 500 MHz): δ 3.84 (d, J = 3.55 Hz, 1H), δ 3.76 (m, 2H), δ 3.70 (m, 2H), and δ 3.52 (m, 1H).^{31}P NMR (D_2O, 500 MHz coupled): 3.01 (t, J = 6.45 Hz). ^{13}C NMR (D_2O, 500 MHz): δ 73.14, δ 70.36, δ 70.07 (d, J = 7.14 Hz), δ 69.69, δ 65.95 (d, J = 5.23 Hz), and δ 62.49.

Insertional Disruption/Deletions of the Genes Encoding RPE, ALSE, and SGCE. We constructed a mutant strain of *E. coli* K-12 in which the genes encoding RPE, ALSE, and SGCE, a third homologue of unknown function, were disrupted (*rpe*, *alse*, and *sgce*). The method described by Datsenko and Wanner (*20*) was used to separately construct disruptions of the three genes in *E. coli* BW25113 by the insertion of genes encoding antibiotic resistance proteins. An *rpe*::kanamycin strain was used to produce a phage P1 lysate that was used to transduce an *alse*::chloramphenicol strain to obtain the double mutant in which the genes encoding both RPE and ALSE had been disrupted. The transduction product was identified by selection on LB plates containing kanamycin and chloramphenicol; the desired junctions were verified by DNA sequence analysis.

The genes encoding the chloramphenicol and kanamycin resistance proteins were eliminated using the pCP20 ampicillin Cam^R plasmid. After testing for loss of antibiotic resistance, the *sgce*::cam strain was used to produce a phage P1 lysate that was used to transduce the strain containing the *rpe* and *alse* disruptions. The transduction product was identified by selection on LB plates containing chloramphenicol; the desired junctions were verified by DNA sequence analysis. This chloramphenicol-resistant strain contains disruptions of the genes encoding RPE, ALSE, and SGCE and was used for purification of the wild type and mutant proteins described in this manuscript.

Cloning, Expression, and Purification of Wild Type ALSE. The gene encoding ALSE (gi:16131911) was PCR-amplified from *E. coli* MG 1655 genomic DNA using Platinum *Pfx* DNA polymerase (Invitrogen). The PCR mixture (100 μL) contained 1 ng of genomic DNA, 10 μL of 10× *Pfx* amplification buffer, 1 mM $MgSO_4$, 0.4 mM concentrations of each of the four deoxynucleoside triphosphates (dNTPs), 40 pmol of each primer, and 2 U of Platinum *Pfx* DNA polymerase. The genes were amplified using a PTC-200 gradient thermal cycler (MJ Research), with the following parameters: 94 °C for 2 min; followed by 40 cycles of 94 °C for 1 min, a gradient annealing temperature range of 45 to 60 °C for 1 min 15 s and 68 °C for 2 min; and a final extension of 68 °C for 10 min. The amplified genes were cloned into the pDMS1a and the pKKHis10 vectors. Both vectors are modifications pKK223-3 vector (Novagen); pDMS1a does not encode an N-terminal His-tag (*21*), and pKKHis10 encodes an N-terminal His_{10}-tag.

Preparation of Wild Type ALSE with an N-Terminal His_{10}-Tag. ALSE with the N-terminal His_{10}-tag was expressed in the strain lacking RPE, ALSE, and SGCE and grown at 37 °C for 30 h in LB containing 100 μg/mL ampicillin and 35 μg/mL chloramphenicol. The cells were collected by centrifugation, resuspended in binding buffer (5 mM imidazole, 0.5 M NaCl, and 20 mM Tris-HCl, pH 7.9), and lysed by sonication. The lysate was applied to a chelating Sepharose Fast Flow column (Pharmacia Biotech) charged with Ni^{2+}. The column was washed with 15% elution buffer (1 M imidazole, 0.5 M NaCl, and 20 mM Tris-HCl, pH 7.9)/85% wash buffer (60 mM imidazole, 0.5 M NaCl, and 20 mM Tris-HCl, pH 7.9), and the protein was eluted with 50% wash buffer/50% strip buffer (100 mM EDTA, 0.5 M NaCl, and 20 mM Tris HCl, pH 7.9). The protein was dialyzed into 10 mM Tris HCl, pH 7.5, containing 150 mM NaCl, concentrated to 30−60 mg/mL by ultrafiltration, and stored at −80 °C.

Construction and Purification of Mutants. The ΔT196, ΔS197 and ΔG198 deletion mutants were constructed by the overlap extension method. The resulting PCR products were digested with *Nde*I and *Bam*HI and ligated into the pDMS1a vector. The plasmids were transformed into the *alse:rpe:sgce*::choramphenicol strain of *E. coli* for expression and purification of the mutant proteins.

Preparation of Wild Type and Mutants of ALSE Reconstituted with Divalent Metal Ions. Wild type and mutants of ALSE without His_{10}-tags were expressed in the strain lacking RPE, ALSE, and SGCE and grown at 20 °C for 30 h in LB with a metal ion supplement (0.5 mM $CoCl_2$, 1 mM $ZnCl_2$, or 1 mM $MnCl_2$), 100 μg/mL ampicillin, and 35 μg/mL chloramphenicol. The cells were collected by centrifugation, resuspended in binding buffer (5% glycerol, 80 μM divalent metal ion, and 20 mM Tris-HCl, pH 7.9), and lysed by sonication. After centrifugation, the lysate was applied to a DEAE-Sepharose FF column. The column was washed with 2.5 column volumes of binding buffer, and the protein was eluted with a linear gradient (from 0 to 50%) of 1 M NaCl in binding buffer. Fractions containing ALSE or its mutants were pooled, and an equal volume of a solution containing 2 M ammonium sulfate, 5% glycerol, 80 μM of the desired divalent metal ion salt, and 20 mM Tris-HCl, pH 7.9. Pooled fractions were then applied to a phenyl-Sepharose column equilibrated with 1 M ammonium sulfate, 5% glycerol, 80 μM of the desired divalent metal ion salt, and 20 mM Tris-HCl, pH 7.9, was added. The column was washed with the 1 M ammonium sulfate-containing buffer, and the protein was eluted with a linear gradient (from 100 to 0%) of the 1 M ammonium sulfate-containing buffer. Fractions containing ALSE or mutants were pooled and dialyzed against a solution containing 5% glycerol, 80 μM of the desired divalent metal ion salt, and 20 mM Tris-HCl, pH 7.9. The dialyzed protein was then purified further with a Source 15Q column, eluted with a linear gradient (from 0 to 50%) of 1 M NaCl in 5% glycerol, 80 μM of the desired divalent metal ion salt, and 20 mM Tris-HCl, pH 7.9. Fractions containing pure protein (>95%) were pooled, concentrated, and dialyzed against 150 mM NaCl, 5% glycerol, 80 μM of the desired divalent metal ion salt, and 20 mM Tris-HCl, pH 7.5, concentrated to 20−63 mg/mL by ultrafiltration, and stored at −80 °C.

Preparation of Metal-Free D-Ribulose 5-Phosphate Epimerase and Reconstitution with Divalent Metal Ions. Metal-free RPE and wild type RPE reconstituted with Zn^{2+} were prepared as previously described (*10*). Wild type RPE reconstituted with Mn^{2+} or Cl^{2+} was similarly prepared except that 20 mM L-glutamate, 20 mM L-arginine, and 20% glycerol were omitted.

Metal Ion Analyses. The procedures used for removing adventitious divalent metal ions from buffers were described previously (*10*). Free or loosely associated metal ions were removed from protein samples by gel filtration using prepacked PD-10 columns (Amersham) that were washed and equilibrated with metal-free 10 mM sodium HEPES, pH 7.5.

Table 1: Data Collection and Refinement Statistics

	ALSE·Mg^{2+}·SO_4	ALSE·Mg^{2+}·D-glucitol 6-phosphate
Data Collection		
wavelength (Å)	0.979	0.979
space group	$P2_12_12_1$	$P2_12_12_1$
mol in au	6	6
unit cell parameters		
a (Å)	75.46	75.71
b (Å)	129.21	129.04
c (Å)	154.45	154.87
resolution (Å)[a]	30−2.50(2.59−2.50)	25.0−2.2(2.28−2.2)
unique reflections	48811	74982
completeness (%)[a]	93.4(92.1)	96.5(92.6)
R_{merge}[a]	0.053(0.246)	0.087(0.039)
average I/σ[a]	40.7(7.6)	14.5(3.1)
Refinement		
resolution (Å)	25−2.5	25−2.2
R_{cryst}	0.222	0.243
R_{free}	0.249	0.265
rmsd, bonds (Å)	0.007	0.007
rmsd, angles (deg)	1.41	1.39
no. of atoms		
protein	10475	10475
water	201	174
Mg^{2+}	6	6
SO_4^{2-}	30	
bound ligand		96
PDB entry	3CT7	3CTL

[a] Numbers in parentheses indicate values for the highest resolution shell.

Inductively coupled plasma emission spectroscopy (ICP) data were obtained by the Garratt-Callahan Company, Burlingame, CA Laboratory as described previously (*10*). Some additional ICP analyses for Zn and Co were performed at the University of Illinois Microanalysis Laboratory.

Coupled-Enzyme Assay of ALSE Activity. The production of D-fructose-6-phopshate from D-allulose 6-phosphate catalyzed by ALSE was quantitated with an irreversible, coupled-enzyme, continuous spectrophotometric assay. The assay (0.2 mL) contained D-allulose 6-phosphate (0.02−7 mM), 0.16 mM $NADP^+$, 4 U of glucose-6-phosphate dehydrogenase (Sigma), 4 U of phosphoglucoisomerase (Sigma), and 150 mM NaCl in 50 mM sodium HEPES, pH 7.5. The change in absorbance at 340 nm was measured as a function of time, with the measured value providing the rate of conversion of D-allulose 6-phosphate to D-fructose 6-phosphate.

Coupled-Enzyme Assay of RPE Activity. RPE was assayed as previously described (*10*).

Polarimetric Assay of RPE Activity. A polarimetric assay was used to avoid divalent metal contamination and also served to verify the coupled-enzyme spectrophotometric assay. The assays were performed as previously described for Zn^{2+}-reconstituted RPE using 80 μM $MnCl_2$, 80 μM $CoCl_2$, or zinc (*10*).

Crystallization and Data Collection. Two different crystal forms (Table 1) were grown by the hanging drop method at room temperature: (1) ALSE, Mg^{2+}, and sulfate, and (2) ALSE, Mg^{2+}, and the substrate analogue D-glucitol 6-phosphate.

For ALSE, Mg^{2+}, and sulfate, the protein solution contained ALSE (60 mg/mL) in 20 mM Tris-HCl, pH 7.9, containing 100 mM NaCl and 5 mM $MgCl_2$; the precipitant contained 16% pentaerythritol ethoxylate, 0.1 M Bis-Tris, pH 6.5, and 50 mM ammonium sulfate. Crystals appeared in 8−9 days and exhibited diffraction consistent with the space group $P2_12_12_1$ with six molecules of ALSE per asymmetric unit.

For ALSE, Mg^{2+}, and the substrate analogue D-glucitol 6-phosphate, the protein solution contained ALSE (30 mg/mL) in 20 mM Tris-HCl, pH 7.9, containing 100 mm NaCl, 5 mM $MgCl_2$, and 20 mM D-glucitol 6-phosphte; the precipitant contained 15% PEG 3350, and 100 mM succinic acid, pH 7.0. Crystals also appeared in 8−9 days and exhibited diffraction consistent with the space group $P2_12_12_1$ with six molecules of ALSE per asymmetric unit.

Prior to data collection, the crystals were transferred to cryoprotectant solution composed of their mother liquid and 20% glycerol and flash-cooled in a nitrogen stream. X-ray diffraction data sets for the complexes with Mg^{2+} and sulfate (Table 1, column 1), and Mg^{2+} and D-glucitol 6-phosphate (column 2) were collected at the NSLS X4A beamline (Brookhaven National Laboratory) on an ADSC CCD detector to 2.5 and 2.2 Å resolution, respectively. Diffraction intensities were integrated and scaled with programs DENZO and SCALEPACK (*22*). The data collection statistics are given in Table 1.

Structure Determination and Model Refinement. The structure of the ALSE·Mg^{2+}·sulfate complex was solved by molecular replacement with the program EPMR (*23*), using the hexamer of RPE from Synechocystis (PDB 1TQJ) as the search model. A single clear solution was found using all data between 15 and 4 Å resolution. Rigid body refinement with CNS (*24*) yielded an electron density map with clear features for a number of amino acid side chains in the ALSE sequence. The bound sulfate anion and Mg^{2+} were clearly visible in electron density maps calculated immediately after the first cycle of rigid body refinement of the protein molecule alone. Iterative cycles of manual rebuilding with TOM (*25*) and refinement with CNS resulted in a model with R_{cryst} and R_{free} 0.222 and 0.249, respectively. The final structure contained 10475 protein atoms, 201 water molecules, 6 Mg^{2+} atoms and 6 sulfate ions for one hexamer in the asymmetric unit. All non-glycine residues lie in allowed regions of the Ramachandran plot.

The structure of the ALSE crystallized with Mg^{2+} and D-glucitol 6-phosphate was determined by molecular replacement using the previous structure as the search model. Iterative cycles of manual rebuilding with TOM and refinement with CNS were performed. The model was refined at 2.2 Å with an R_{cryst} of 0.243 and an R_{free} of 0.265. The structure contained a well-defined Mg^{2+} and D-glucitol 6-phosphate in each polypeptide of the hexamer.

Final crystallographic refinement statistics are provided in Table 1.

RESULTS AND DISCUSSION

As described in the introductory comments, the genomes of species of *E. coli* encode a catabolic pathway for the rare hexose D-allose that includes ALSE, a homologue of RPE (Scheme 2) (*16*). The structurally characterized RPE from *S. pyogenes* and the ALSE from *E. coli* K-12 share 39% sequence identity. On the basis of the sequence alignment (Figure 2), the active site of ALSE is predicted to contain homologues of the ligands for an essential divalent metal ion that are found in RPE, His 30, His 63, Asp 32, and Asp

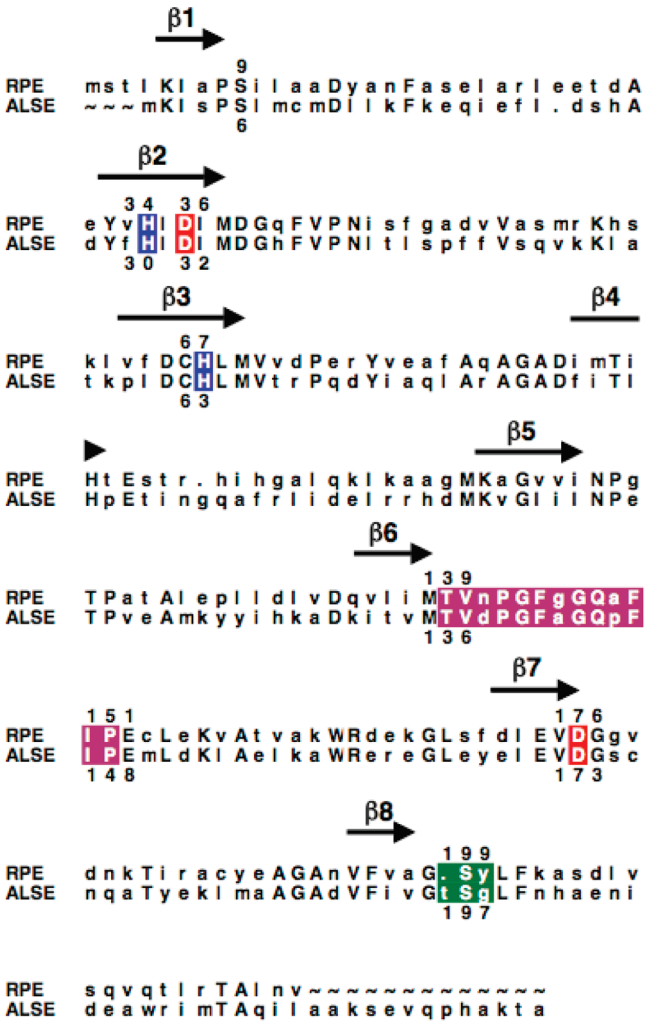

FIGURE 2: Sequence alignment of the RPE from *S. pyogenes* and the ALSE from *E. coli* K-12. The positions of the β-strands in the $(\beta/\alpha)_8$-barrel are marked with arrows; conserved residues are designated with capital letters. The His residues that coordinate the essential divalent metal ion are highlighted in blue, and the Asp residues that are the acid/base catalysts in the 1,1-proton transfer reactions are highlighted in red. The residues in the phosphate binding motifs are highlighted in green, and active site loops are highlighted in magenta.

173, thereby allowing a conserved mechanism for the 1,1-proton transfer reaction.

However, the structural bases for differences in substrate specificity are not as readily predicted from the sequence alignment. Three amino acid substitutions appear to distinguish the active site loops in ALSE and RPE that sequester the bound substrate from the solvent (Asn to Asp at residue 138, Gly to Ala at residue 142, and Ala to Pro at residue 145 in ALSE). But, the side chains of these residues are solvent-exposed in RPE and, therefore, cannot be responsible for differences in substrate specificity. However, the loop that follows the eighth β-strand in the phosphate binding motif is predicted to contain an additional residue. Thus, we were intrigued by structural basis for the presumed different substrate specificities of RPE and ALSE and sought a structural explanation for this difference.

Initial Functional Characterization of ALSE. In the pathway for D-allose utilization, the binding/transport protein for D-allose has been structurally characterized (*26, 27*) and D-allose kinase (AlsK, Scheme 2) has been kinetically

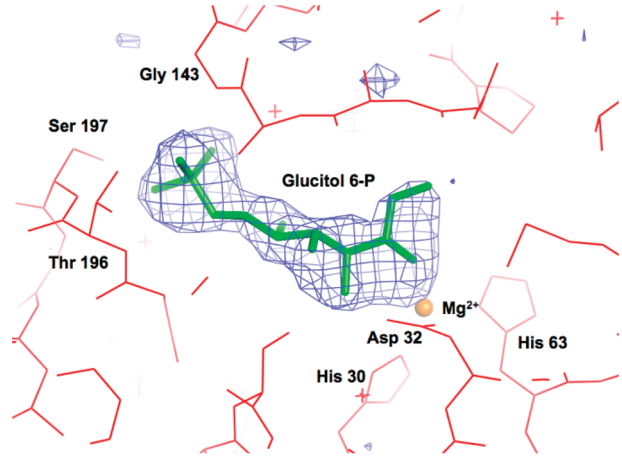

FIGURE 3: Omit electron density map ($F_o - F_c$) of the D-glucitol 6-phosphate ligand contoured at 3σ. D-Glucitol 6-phosphte was omitted from the model, and the remainder of the unit cell was subjected to a cycle of simulated annealing with CNS at 3000 °C.

characterized (*17, 18*). But ALSE had not been isolated and characterized. We cloned the gene encoding the ALSE from *E. coli* K-12 with an N-terminal His_{10}-tag and initially purified the protein using a Ni^{2+}-chelating column without regard to its metal ion content (determined by ICP as variable, substoichiometric amounts of Mg^{2+} and trace amounts of Fe^{2+}, Mn^{2+}, Ni^{2+}, and Zn^{2+}). Structures of this protein were determined in the presence of Mg^{2+} as well as either sulfate anion or D-glucitol 6-phosphate, an inert analogue of D-fructose 6-phosphate (*vide infra*). However, minimal ALSE activity was detected in the coupled-enzyme spectrophotometric assay (k_{cat}, 0.14 s^{-1}; k_{cat}/K_m, 8 M^{-1} s^{-1}). Given our experiences with RPE, we suspected that the low activity could be explained by the requirement for a "missing" transition metal ion: when the His-tagged RPE from *S. pyogenes* was isolated using a Ni^{2+}-chelating column, the enzyme displayed reduced catalytic activity until adventitious metal ions were removed by incubation with EDTA and Zn^{2+} was added (*10*).

Divalent Metal Ion Requirements for ALSE and RPE. We also were concerned that the low activity could result from the N-terminal His_{10}-tag competing for metal ions. Because we could not cleave the tag with thrombin, we expressed and purified ALSE without the affinity tag. But, when this protein was isolated by successive DEAE-anion exchange, phenyl-Sepharose reverse-phase, and Resource-Q anion exchange chromatographies, it also had low ALSE activity.

If the growth medium and buffers for purification were supplemented with $ZnCl_2$, the protein without the tag displayed greater levels of ALSE activity; ICP analysis revealed the presence of 0.66 equiv of Zn (Table 2). Although Zn was substoichiometric, we hypothesized that other transition metal ions might provide greater activity. Therefore, we analogously expressed and purified ALSE in the presence of either $MnCl_2$ or $CoCl_2$. These proteins also displayed enhanced values for their kinetic constants, with Co^{2+} providing the greatest level of activity; both proteins contained near stoichiometric amounts of the added metal (Table 2). We used Co^{2+}-containing wild type and mutant enzymes for the remainder of our studies.

Given the preference of ALSE for Co^{2+}, we re-examined the metal ion requirement for the RPE from *S. pyogenes*.

Table 2: Kinetic Parameters, Substrate Specificities, and Metal Contents for Wild Type RPE and ALSE

	Co-ALSE	Mn-ALSE	Zn-ALSE	Co-RPE	Mn-RPE	Zn-RPE
			RPE[a]			
k_{cat} (s^{-1})	2 ± 0.8	*b*	*b*	3,800 ± 160	1,600 ± 70	500 ± 20
K_m (mM)	3.0 ± 0.3	*b*	*b*	1.2 ± 0.1	2.2 ± 0.3	3.2 ± 0.2
k_{cat}/K_m (M^{-1} s^{-1})	670	190	390	3,200,000	7,100	1,500
			ALSE[a]			
k_{cat} (s^{-1})	46 ± 4	7.3 ± 0.5	2.2 ± 0.2	0.016 ± 0.002	0.012 ± 0.001	0.011 ± 0.001
K_m (mM)	1.6 ± 0.4	1.1 ± 0.2	3.3 ± 0.4	1.1 ± 0.3	1.1 ± 0.06	1.8 ± 0.4
k_{cat}/K_m (M^{-1} s^{-1})	29,000	6,600	700	14	11	6
			Substrate Specificity (RPE/ALSE)[c]			
RPE/ALSE	0.025	0.029	0.6	230,000	64,000	25,000
			Metal Content[d]			
Co	0.99	0	0	1.46	0	0
Zn	0	0.15	0.66	0.11	0.17	1.15
Mn	0	0.94	0	0	0.98	0

[a] Using the spectrophotometric assay described in Materials and Methods. [b] Could not saturate with substrate; k_{cat}/K_m was determined by the dependence of velocity on substrate concentration. [c] $(k_{cat}/K_m)_{RPE}/(k_{cat}/K_m)_{ALSE}$. [d] Stoichometry of metal to protein; metal content determined by ICP as described in Materials and Methods.

We previously reported that the RPE was activated by Zn^{2+} but did not examine whether it also could be activated by either Mn^{2+} or Co^{2+}. We followed our published procedure for preparing metal-free RPE and reconstituted it with Mn^{2+} or Co^{2+}. The RPE also is maximally activated by Co^{2+}, with Mn^{2+} also providing more activity than previously reported for Zn^{2+} (Table 2).

Promiscuity of ALSE for the RPE Reaction and Vice Versa. We assayed the various transition metal ion-reconstituted samples of ALSE for RPE activity and analogous samples of RPE for ALSE activity. ALSE was promiscuous for the RPE reaction, and *vice versa* (Table 2). On the basis of the values of k_{cat}/K_m (the specificity constant), ALSE is more promiscuous than RPE. Focusing on the most active Co-containing epimerases, the ratio of the values for k_{cat}/K_m (RPE:ALSE) is 0.023 for ALSE and 2.3×10^5 for RPE.

Structure of ALSE. We determined structures of the low activity, N-terminal His-tagged ALSE in the presence of 5 mM Mg^{2+} and either (1) sulfate anion at 2.5 Å resolution or (2) D-glucitol 6-phosphate, an inert structural analogue of the D-fructose 6-phosphate product, at 2.2 Å resolution (Figure 3). Unfortunately, we were unable to obtain any crystals of ALSE without the His-tag that had been reconstituted with Zn^{2+}, Mn^{2+}, or Co^{2+}. Because the sample of ALSE used to obtain these crystals contained some Mg^{2+} but essentially no transition metal ions as assessed by ICP analyses (*vide supra*), we assign Mg^{2+} to the electron density to which O2 and O3 of the analogue are coordinated. Although the protein used to obtain crystals had low levels of ALSE activity, we believe that the structures of the complexes can be used to infer the structural bases for substrate specificity, the focus of this study, given (1) the excellent superposition of the sulfate/phosphate binding motifs at the ends of the seventh and eighth β-strands in the two complexes and (2) the global similarity of the structures of these complexes to the structure of RPE liganded with Zn^{2+} and D-xylitol 5-phosphate (*10*).

In each structure, the asymmetric unit contains six polypeptides. These are arranged as trimers of dimers to form hexamers; we reported a similar hexameric structure for the homologous RPE from *S. pyogenes* (*10*). Like RPE, ALSE is a $(\beta/\alpha)_8$-barrel, with the active site located at the C-terminal ends of the β-strands.

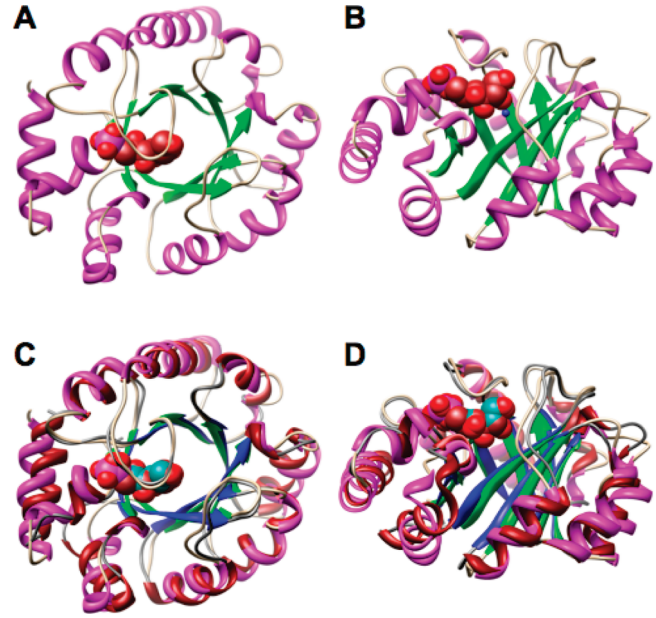

FIGURE 4: Structures of the polypeptides of ALSE and RPE. Panels A and B, the D-glucitol 6-phosphate-liganded complex of ALSE: panel A, view from the C-terminal ends of the β-strands of the $(\beta/\alpha)_8$-barrel domains; panel B, view from the sides of the $(\beta/\alpha)_8$-barrel domains. Panels C and D, the D-glucitol 6-phosphate-liganded complex of ALSE superimposed on the D-xylitol 5-phosphate-liganded complex of RPE (*10*): panel C, view from the C-terminal ends of the β-strands of the $(\beta/\alpha)_8$-barrel domains; panel D, view from the sides of the $(\beta/\alpha)_8$-barrel domains. In ALSE, the backbone is shown in tan, the β-strands are shown in green, the α-helices are shown in magenta, and the D-glucitol 6-phosphate ligand is shown in brown. In RPE, the backbone is shown in gray, the β-strands are shown in blue, and α-helices are shown in red, and the D-xylitol 5-phosphate ligand is shown in dark cyan.

The structure of a polypeptide of ALSE liganded with D-glucitol 6-phosphate and its superposition with a polypeptide of RPE liganded with D-xylitol 5-phosphate are shown in Figure 4. Like RPE, a loop that follows the sixth β-strand sequesters the active site of ALSE from the solvent. As expected based on the sequence alignment (Figure 2), the polypeptides are well-superimposed (rmsd 1.05 Å for 168 pairs of α-carbons).

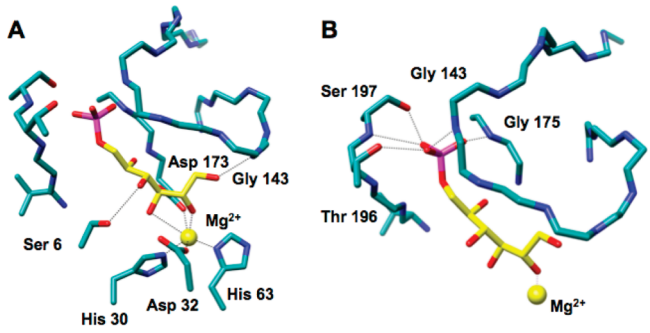

FIGURE 5: The active site of ALSE. Panel A, the interactions of the substrate analogue D-glucitol 6-phosphate (yellow) with the active site. Panel B, the interactions of the phosphate group of D-glucitol 5-phosphate with the phosphate binding motif (Thr 196 and Ser 197) and the active site loop (Gly 143). A 3.2 Å threshold was used for drawing hydrogen bonding and liganding interactions.

Active Site of ALSE. The structure of the active site of the D-glucitol 6-phosphate-liganded ALSE (Figure 5) is similar to that of the D-xylitol 5-phosphate-liganded RPE (Figure 1): the positions of the metal ions, their protein-derived ligands, and the 2- and 3-OH groups of D-glucitol 6-phosphate in ALSE and of D-xylitol 5-phosphate in RPE superimpose closely, as would be expected from mechanistically conserved geometric requirements for the "same" 1,1-proton transfer reactions involving ketose substrates. Therefore, in analogy to the structure−function relationships we determined for RPE (*10*), we propose that Asp 32 is the D-allulose 6-phosphate specific acid/base catalyst and Asp 173 is the D-fructose 6-phosphate specific acid/base catalyst in the ALSE-catalyzed 1,1-proton transfer reaction.

With these conserved geometric features, the phosphate groups must occupy different positions as a consequence of the differing lengths of the substrates. As suggested by the sequence alignment (Figure 2), the loop following the eighth β-strand in ALSE has an additional residue so that it can accommodate the longer hexulose 6-phosphate substrates for the ALSE-catalyzed reaction (Figure 5). The phosphate group of D-glucitol 6-phosphate makes several hydrogen-bonding contacts with the expanded phosphate binding motif in the C-terminal $(\beta/\alpha)_2$-quarter barrel: the amide of Ser 175 at the end of seventh β-strand, the amide of Thr 196 at the end of the eighth β-strand, and the OH groups of both Thr 196 and Ser 197. In addition, the phosphate group also forms a hydrogen bond with the amide of Gly 143 in the closed active site loop.

The locations of the backbone and side chain hydrogen bond donors in the loop following the eighth β-strand of ALSE are displaced from those in RPE as permitted by the insertion of a single amino acid residue at this position in the sequence of ALSE (Figure 6). As a result, the active site of RPE sterically should be unable to accommodate the longer substrate for the ALSE reaction, but the active site of ALSE should be able to accommodate the shorter substrate for the RPE reaction. These predictions are in accord with the experimentally measured substrate promiscuities (Table 2): the ratio of the values for k_{cat}/K_m (RPE:ALSE) is 0.023 for ALSE and 2.3×10^5 for RPE.

Deletion Mutants of the Phosphate Binding Motif of ALSE. Given the differences in both the substrate specificities and structures of the phosphate binding motifs in ALSE and RPE, we examined the consequences of contracting the phosphate

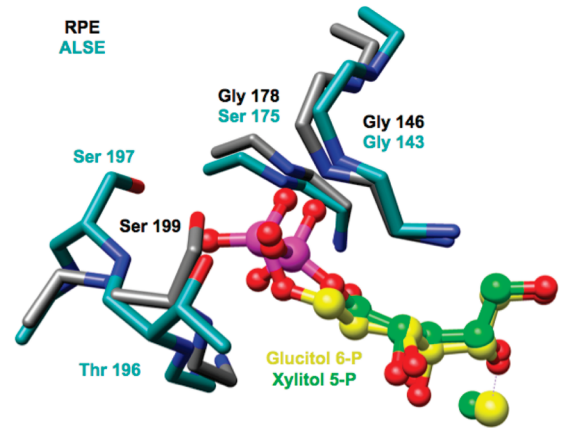

FIGURE 6: A superposition of the phosphate binding motifs in RPE (gray) and ALSE (cyan). In RPE the D-xylitol 5-phosphate ligand is shown in green; in ALSE, the D-glucitol 6-phosphate ligand is shown in yellow.

binding motif in ALSE and, thereby, allowing it to assume the conformation of the motif in RPE. We constructed three mutants in which one of the residues in the loop following the eighth β-strand is deleted, ΔT196, ΔS197 and ΔG198, thereby reducing the length to that found in RPE (Figure 2). In each mutant, the position of the backbone amide that hydrogen bonds to the phosphate group of the substrate (residue 196, Thr in wild type) should be altered; in addition, in the ΔT196 and ΔS197 mutants, one of the side chain OH groups that hydrogen bonds to the phosphate group is missing.

The mutants were expressed and purified so that Co^{2+} would be present in the active site; when assayed for ALSE activity, the values of k_{cat}/K_m were modestly reduced for all three mutants (Table 3). In contrast, when assayed for RPE activity, the values of k_{cat}/K_m were significantly increased. As a result, the promiscuity for the RPE reaction was increased for all three mutants, such that D-ribulose 5-phosphate was the preferred substrate (RPE:ALSE = 5.2, 7.8, and 4.3 for the ΔT196, ΔS197 and ΔG198 mutants, respectively). However, for all three mutants the values for k_{cat} and k_{cat}/K_m for the RPE reaction remained less than those for the RPE from *S. pyogenes.*

For both activities, the changes in specificity are dominated by changes in the values of k_{cat} (Table 3). We were not able to determine the structures of any of the mutants, so a structure-based explanation for the changes in their substrate specificities is not possible. However, the structures of RPE liganded with D-xylitol 5-phosphate and ALSE liganded with D-glucitol 6-phosphate reveal hydrogen bonding interactions not only between the phosphate monoester dianions and the binding motif in the C-terminal $(\beta/\alpha)_2$-quarter barrel but also with the active site loops (the amides of Gly 146 and Gly 143, respectively). This is reminiscent of the interactions of the phosphate groups of the substrates in the active sites of TIM (*13*) and OMPDC (*14*) with their active site loops. For both TIM (*11*) and OMPDC (*12*), Amyes and Richard proposed that the active site loops transmit the energy obtained by binding the phosphate group to catalysis, given that phosphite "allosterically" activates both enzymes for utilization of desphospho-truncated substrates.

Thus, the significant increases in the values of k_{cat} for the RPE reaction (>100-fold) that dominate the change in

Table 3: Kinetic Parameters, Substrate Specificities, and Metal Contents for Co-Reconstituted Wild Type ALSE, ALSE Mutants, and Wild Type RPE

	Co-ALSE	Co-ΔT196	Co-ΔS197	Co-ΔG198	Co-RPE
			RPE[a]		
k_{cat} (s^{-1})	2 ± 0.8	130 ± 7	240 ± 14	440 ± 20	3800 ± 160
K_m (mM)	3.0 ± 0.3	3.9 ± 0.5	2.8 ± 0.6	5.1 ± 0.5	1.2 ± 0.1
k_{cat}/K_m (M^{-1} s^{-1})	670	33,000	85,000	86,000	3,200,000
			ALSE[a]		
k_{cat} (s^{-1})	46 ± 4	7.5 ± 0.3	12 ± 0.8	34 ± 2	0.016 ± 0.002
K_m (mM)	1.6 ± 0.4	1.2 ± 0.1	1.1 ± 0.2	1.7 ± 0.2	1.1 ± 0.3
k_{cat}/K_m (M^{-1} s^{-1})	29,000	6,300	11,000	20,000	14
			Substrate Specificity (RPE/ALSE)[b]		
RPE/ALSE	0.023	5.2	7.8	4.3	230,000
			Metal Content[c]		
Co	0.99	1.00	0.95	1.11	1.46
Zn	0	0	0	0	0.11

[a] Using the spectrophotometric assay described in Materials and Methods. [b] $(k_{cat}/K_m)_{RPE}/(k_{cat}/K_m)_{ALSE}$. [c] Stoichometry of metal to protein; metal content determined by ICP as described in Materials and Methods.

specificity from D-allulose 6-phosphate to D-ribulose 5-phosphate in the mutants likely reflect the ability of the altered binding site to better couple phosphate binding with catalysis *via* ligand-induced changes in the structure of the active site, including the loop at the end of the sixth β-strand (*15*). Similarly, the small decreases in the values of k_{cat} for the ALSE reaction (<6-fold) likely result from less efficient utilization of the intrinsic binding energy of the phosphate group. Indeed, the values of both k_{cat} and k_{cat}/K_m for the RPE reaction catalyzed by the RPE from *S. pyogenes* are larger than those for the ALSE reaction catalyzed by ALSE, suggesting that the mechanism for coupling the phosphate binding energy to catalysis has not been optimized in the ALSE-catalyzed reaction.

That this mechanism for determining substrate specificity is more "sophisticated" than "simple" discrimination of the substrates based on their affinities supports the hypothesis that the evolution of function in $(\beta/\alpha)_8$-barrels that contain the conserved phosphate binding motif has been perfected to optimally utilize the intrinsic binding energy to assist catalysis. Presumably, as in TIM and OMPDC, this coupling involves the active site loop that sequesters the substrate from solvent and productively orients the substrate *vis-à-vis* the active site functional groups.

CONCLUSIONS

The members of the ribulose-phosphate binding $(\beta/\alpha)_8$-barrel "superfamily" share a conserved phosphate binding motif formed by the C-terminal $(\beta/\alpha)_2$-quarter barrel (*10*). The differing substrate specificities for the 1,1-proton transfer reactions catalyzed by the homologous RPE (pentulose 5-phosphate substrates) and ALSE (hexulose 6-phosphate substrates) are associated with the differing structures of their phosphate binding motifs; in ALSE with the longer substrate, the loop following the eighth β-strand contains an additional residue that increases the distance of the binding site for the phosphate moiety from the active site residues. ALSE is naturally promiscuous for the RPE reaction. That the promiscuity is enhanced, i.e., the substrate specificity is reversed, by deletions of residues in the phosphate binding motif in ALSE, suggests that the phosphate binding motif not only participates in "gripping" the substrate but also plays an essential role in transmitting the energy derived from occupancy of the motif to catalysis *via* its interactions with the conformationally flexible active site loop that sequesters the substrate from solvent.

REFERENCES

1. Nagano, N., Orengo, C. A., and Thornton, J. M. (2002) One fold with many functions: the evolutionary relationships between TIM barrel families based on their sequences, structures and functions. *J. Mol. Biol. 321*, 741–765.
2. Sterner, R., and Hocker, B. (2005) Catalytic versatility, stability, and evolution of the $(\beta/\alpha)_8$-barrel enzyme fold. *Chem. Rev. 105*, 4038–4055.
3. Lang, D., Thoma, R., Henn-Sax, M., Sterner, R., and Wilmanns, M. (2000) Structural evidence for evolution of the β/α barrel scaffold by gene duplication and fusion. *Science 289*, 1546–1550.
4. Hocker, B., Beismann-Driemeyer, S., Hettwer, S., Lustig, A., and Sterner, R. (2001) Dissection of a $(\beta/\alpha)_8$-barrel enzyme into two folded halves. *Nat. Struct. Biol. 8*, 32–36.
5. Bork, P., Gellerich, J., Groth, H., Hooft, R., and Martin, F. (1995) Divergent evolution of a beta/alpha-barrel subclass: detection of numerous phosphate-binding sites by motif search. *Protein Sci. 4*, 268–274.
6. Hocker, B., Schmidt, S., and Sterner, R. (2002) A common evolutionary origin of two elementary enzyme folds. *FEBS Lett. 510*, 133–135.
7. Henn-Sax, M., Hocker, B., Wilmanns, M., and Sterner, R. (2001) Divergent evolution of $(\beta/\alpha)_8$-barrel enzymes. *Biol. Chem. 382*, 1315–1320.
8. Gerlt, J. A. (2000) New wine from old barrels [news]. *Nat. Struct. Biol. 7*, 171–173.
9. Nicolet, Y., and Drennan, C. L. (2004) AdoMet radical proteins-from structure to evolution-alignment of divergent protein sequences reveals strong secondary structure element conservation. *Nucleic Acids Res. 32*, 4015–4025.
10. Akana, J., Fedorov, A. A., Fedorov, E., Novak, W. R., Babbitt, P. C., Almo, S. C., and Gerlt, J. A. (2006) D-Ribulose 5-phosphate 3-epimerase: functional and structural relationships to members of the ribulose-phosphate binding (beta/alpha)8-barrel superfamily. *Biochemistry 45*, 2493–2503.
11. Amyes, T. L., O'Donoghue, A. C., and Richard, J. P. (2001) Contribution of phosphate intrinsic binding energy to the enzymatic rate acceleration for triosephosphate isomerase. *J. Am. Chem. Soc. 123*, 11325–11326.
12. Amyes, T. L., Richard, J. P., and Tait, J. J. (2005) Activation of orotidine 5′-monophosphate decarboxylase by phosphite dianion: the whole substrate is the sum of two parts. *J. Am. Chem. Soc. 127*, 15708–15709.
13. Davenport, R. C., Bash, P. A., Seaton, B. A., Karplus, M., Petsko, G. A., and Ringe, D. (1991) Structure of the triosephosphate isomerase-phosphoglycolohydroxamate complex: an analogue of the intermediate on the reaction pathway. *Biochemistry 30*, 5821–5826.

14. Appleby, T. C., Kinsland, C., Begley, T. P., and Ealick, S. E. (2000) The crystal structure and mechanism of orotidine 5′-monophosphate decarboxylase. *Proc. Natl. Acad. Sci. U.S.A. 97* 2005–2010.
15. Morrow, J. R., Amyes, T. L., and Richard, J. P. (2008) Phosphate Binding Energy and Catalysis by Small and Large Molecules. *Acc. Chem. Res. 41*, 539–548.
16. Kim, C., Song, S., and Park, C. (1997) The D-allose operon of Escherichia coli K-12. *J. Bacteriol. 179*, 7631–7637.
17. Larion, M., Moore, L. B., Thompson, S. M., and Miller, B. G. (2007) Divergent evolution of function in the ROK sugar kinase superfamily: role of enzyme loops in substrate specificity. *Biochemistry 46*, 13564–13572.
18. Miller, B. G., and Raines, R. T. (2005) Reconstitution of a defunct glycolytic pathway via recruitment of ambiguous sugar kinases. *Biochemistry 44*, 10776–10783.
19. Ames, B. N. (1966) Assay of Inorganic Phosphate, Total Phosphate and Phosphatases. *Methods Enzymol 8*, 115–118.
20. Datsenko, K. A., and Wanner, B. L. (2000) One-step inactivation of chromosomal genes in *Escherichia coli* K-12 using PCR products. *Proc. Natl. Acad. Sci. U.S.A. 97*, 6640–6645.
21. Schmidt, D. M., Hubbard, B. K., and Gerlt, J. A. (2001) Evolution of Enzymatic Activities in the Enolase Superfamily: Functional Assignment of Unknown Proteins in Bacillus subtilis and Escherichia coli as L-Ala-D/L-Glu Epimerases. *Biochemistry 40*, 15707–15715.
22. Otwinowski, Z., and Minor, W. (1997) Processing of X-ray diffraction data collected in oscillation mode, in *Methods in Enzymology* (Carter, C. W. J., Sweet, R. M., Abelson, J. N., and Simon, M. I., Eds.) pp 307−326, Academic Pres, New York.
23. Kissinger, C. R., Gehlhaar, D. K., and Fogel, D. B. (1999) Rapid automated molecular replacement by evolutionary search. *Acta Crystallogr., Sect. D: Biol. Crystallogr. 55*, 484–491.
24. Brunger, A. T., Adams, P. D., Clore, G. M., DeLAno, W. L., Gros, P., Grosse-Kunstleve, R. W., Jiang, J. S., Kuszewski, J., Nilges, M., Pannu, N. S., Read, R. J., Rice, L. M., Simonson, T., and Warren, G. L. (1998) Crystallography & NMR system: A new software suite for macromolecular structure determination. *Acta Crystallogr. D54*, 905–921.
25. Jones, A. T. (1985) Interactive computer graphics: FRODO. *Methods Enzymol. 115*, 157–171.
26. Magnusson, U., Chaudhuri, B. N., Ko, J., Park, C., Jones, T. A., and Mowbray, S. L. (2002) Hinge-bending motion of D-allose-binding protein from Escherichia coli: three open conformations. *J. Biol. Chem. 277*, 14077–84.
27. Chaudhuri, B. N., Ko, J., Park, C., Jones, T. A., and Mowbray, S. L. (1999) Structure of D-allose binding protein from Escherichia coli bound to D-allose at 1.8 A resolution. *J. Mol. Biol. 286*, 1519–31.

BI800821V